JOURNAL OF CATALYSIS 71, 99–110 (1981)

X-Ray Photoelectron Spectroscopic Study of Mixed Oxide Catalysts Containing Molybdenum

I. SnO_2–MoO_3 Catalysts

YASUAKI OKAMOTO, KENJI OH-HIRAKI, TOSHINOBU IMANAKA, AND SHIICHIRO TERANISHI

Department of Chemical Engineering, Faculty of Engineering Science, Osaka University, Toyonaka, Osaka 560, Japan

Received January 21, 1981; revised April 29, 1981

SnO_2–MoO_3 mixed oxide catalysts were characterized by X-ray photoelectron spectroscopy coupled with ESR, ir, Mössbauer, and X-ray diffraction analysis. The dehydrogenation and dehydration activities of the catalysts for *sec.*-butyl alcohol were measured at 190°C in an air stream. As for the surface composition of the catalysts calcined at 550°C, the surface enrichment of Mo was observed in the region of Mo/Mo + Sn < 0.75 and that of Sn in the other region. On the basis of the catalytic properties, SnO_2–MoO_3 catalysts can be classified into two groups; catalyst I with the surface composition of Mo/Mo + Sn < 0.5 and catalyst II with that of Mo/Mo + Sn > 0.5. In the former catalyst group, when contacted with alcohols, Mo(VI) was found to be easily reduced to Mo(V), which was stable against a H_2 treatment at 400°C. With catalyst II, it was revealed that on contact with alcohols, Mo(VI) was relatively difficult to reduce to lower valence states and that part of Mo(VI) was easily reduced to Mo(IV) by the H_2 treatment. These results suggest that the reactivities of lattice oxygen are enhanced by combining SnO_2 and MoO_3 and that the activation modes of lattice oxygen and the catalytic properties of activated lattice oxygen are significantly altered with the composition of the catalyst. A surface model of SnO_2–MoO_3 catalysts is proposed on the basis of these results.

INTRODUCTION

It is well known that multicomponent oxide catalysts show much better catalytic activity and selectivity than the component oxide catalysts in a variety of reactions. However, the roles of the component oxides in the reactions are not fully understood. This is due to the lack of the knowledge on the surface state of the catalysts, such as surface composition, chemical states of component oxides, and surface structure, particularly during the reactions. To characterize the surface state of the catalysts, X-ray photoelectron spectroscopy (XPS) has already been found to be an excellent technique, since it provides invaluable information on the surface layers of solid materials. For instance, it has been demonstrated by using XPS that the catalytic activity and selectivity correlate strongly to the surface composition of the catalysts for Sn–Mo (*1*), Sn–Zr (*2*), Bi–Mo (*3*), and Sn–Sb (*4, 5*) mixed oxide catalysts. According to thermodynamic considerations (*6*), the surface composition must be different from the bulk one. Cimino and his co-workers (*7*) demonstrated clearly these phenomena for the Mg–Zn oxide system. Such XPS evidence has been accumulated for several catalyst systems (*1–5, 8–12*). Of particular interest are the changes in the surface composition of the catalysts and in the chemical states of the component oxides with various treatments and reactions (*1, 9, 13–15*). XPS information on the dynamic behavior of the catalyst surface is rapidly increasing now. In this report, surface characterization of SnO_2–MoO_3 catalysts was conducted utilizing

0021-9517/81/090099-12$02.00/0

XPS and compared with catalytic activity and selectivity for *sec.*-butyl alcohol conversions.

SnO_2–MoO_3 catalysts show high activities and selectivities for partial oxidations, such as the oxidations of propylene to acrolein (*16, 17*) and to acetone in the presence of H_2O (*18–24*), butene to butadiene (*25*), butadiene to maleic anhydride (*25*), and methyl alcohol to formaldehyde (*26*). In SnO_2–MoO_3 catalysts, SnO_2 shows high deep oxidation activities, while MoO_3 is selective, although its activity is relatively low. Combination of these component oxides leads to higher activities and selectivities for partial oxidations as observed for other mixed oxide catalysts. However, the roles played by Sn and Mo in catalysis have not been well understood. On the basis of the Mössbauer study on Sn, Margolis (*17*) suggested redox cycles including Sn(II)–Sn(IV) and Mo(VI)–Mo(V) for the oxidation of olefins. On the other hand, Niwa *et al.* (*26*) proposed a Mo(V)–Mo(IV) redox cycle for the methyl alcohol oxidation by using ESR. Takita *et al.* (*19*) and Ai (*25, 27*) stressed the importance of the acid–base properties of the catalysts. Surface characterization of SnO_2–MoO_3 catalysts by XPS would shed important light on the behavior of Sn and Mo, since XPS provides the chemical states of both Sn and Mo, in contrast to ESR and Mössbauer. The XPS results were combined here with complementary techniques; ESR, ir, XRD, and Mössbauer spectroscopy.

We carried out the reaction of *sec.*-butyl alcohol in an air stream over SnO_2–MoO_3 catalysts having various compositions, since (oxidative) dehydrogenation to methylethylketone and dehydration to butenes would provide information both on the oxidation activity and on solid acid–base properties. Reductions of the catalyst with several kinds of alcohol and H_2 were also investigated to reveal the redox behavior of the catalyst and the reaction mechanism of the oxidative dehydrogenation of alcohols.

EXPERIMENTAL

Catalysts

SnO_2–MoO_3 catalysts were prepared using stannous chloride and ammonium paramolybdate. The tin hydroxide precipitate obtained by adding an aqueous ammonium solution was filtered and washed with distilled water. Required amounts of an aqueous ammonium paramolybdate solution were added to the precipitate to obtain Sn–Mo oxide catalysts with desired Sn/Mo ratio, followed by evaporation to dryness at 90°C, drying at 110°C for 16 h, and calcining at 550°C for 5 h in air. Pure SnO_2 was obtained by the same procedures except for the addition of ammonium paramolybdate. Pure MoO_3 was prepared by evaporating an aqueous ammonium paramolybdate solution to dryness, followed by the same procedure as for the catalysts. All the catalysts were used in fine powders as prepared.

Procedures

(*1*) *Catalytic conversion of sec.-butyl alcohol.* The reaction of *sec.*-butyl alcohol (2-BA) was carried out over the SnO_2–MoO_3 catalysts at 190°C in a dry-air stream using a conventional fixed-bed flow reactor in a differential mode (2-BA/O_2; 1.16, air flow rate; 18 ml/min). The alcohol was fed into the air stream by utilizing a mechanically controlled microfeeder. The products were methylethylketone (MEK), butenes, and a small amount of di-*sec.*-butyl ether. The formations of carbon oxides were not detected. All the products were analyzed by gas chromatography. A steady-state activity was attained after ca. 30 min and usually measured at 1.5-h reaction time.

(*2*) *XPS measurements.* X-Ray photoelectron spectra of the catalysts were measured at room temperature on a Hitachi 507 photoelectron spectrometer using Al$K\alpha$ radiation (50 mA, 10 kV). The catalyst samples were mounted on double-sided adhesive tape. All the binding energies were referenced to the C_{1s} level (285.0 eV) of contaminant carbon. The accuracy in the

determination of the binding energy values was within ±0.2 eV. The XPS peak area intensities were measured by planimetry of the graphic displays of the spectra by assuming linear baselines. Mechanical mixtures of the pure SnO_2 and MoO_3 catalysts were used to obtain relative atomic sensitivities of $Sn_{3d_{5/2}}$ and Mo_{3d} levels. From a linear correlation between $Mo_{3d}/Sn_{3d_{5/2}}$ peak area intensity ratios and Mo/Sn atomic ratios, the atomic sensitivity ratio of 0.52 was obtained, this value being in good agreement with 0.59 reported by Wagner (*28*). The surface composition of the catalyst was calculated by using the atomic sensitivity ratio thus obtained.

The X-ray photoelectron spectra of the catalysts which had reached steady states or which had been reduced with alcohols or hydrogen were measured without exposing the catalysts to air or moisture using a N_2-filled glovebox. The detailed procedures were described elsewhere (*29*).

(*3*) *Other procedures.* ESR spectra of the catalysts were measured in the *X*-band at room temperature using a JEOL spectrometer (JES-ME-1X). Reduction of the SnO_2–MoO_3 catalysts with 10 Torr of 2-BA and subsequent oxidation with ca. 150 Torr of O_2 were carried out using an *in situ* cell with a sidearm for ESR measurements.

To examine the properties of Mo oxide in the catalyst, the ir intensity of Mo=O band (990 cm^{-1}) was measured (Hitachi grating infrared spectrometer, EPI-G). The absorption intensities of the Mo=O band were normalized for the strong signal (ν_1; 1100 cm^{-1}) of $MgCO_3$ which was mechanically mixed with the catalyst (catalyst/$MgCO_3$ = 2/1 by weight) as a standard. Mixed samples were pressed into disks using KBr powder.

X-Ray diffraction analyses of the catalysts were carried out using a Cu anode with a Ni filter (Shimazu VD-1). To obtain relative crystallinities of MoO_3 and SnO_2, mechanical mixtures of silicon and the catalysts were used and peak area intensities due to silicon (2θ = 28.4°), MoO_3 (25.5°), and SnO_2 (26.5°) were obtained. No new XRD peak was observed, indicating the absence of definite Sn–Mo mixed oxide compounds.

Mössbauer spectra of Sn were obtained using ^{119m}Sn in $CaSnO_3$ at room temperature. The spectra of reduced catalysts were obtained by covering the samples with epoxy resin in the N_2-filled glovebox to prevent the reduced catalysts from contact with air.

The BET surface areas of the catalysts were measured at 77 K using N_2 after evacuating the catalysts at 300°C for 1 h. They are summarized in Table 1.

RESULTS AND DISCUSSION

Shown in Fig. 1 are the X-ray photoelectron spectra of the Mo_{3d}, $Sn_{3d_{5/2}}$, and Sn $M_4N_{4,5}N_{4,5}$ Auger levels for the calcined catalysts. The binding energies of the $Mo_{3d_{5/2}}$ and $Sn_{3d_{5/2}}$ bands were 233.1 and 486.9 eV, respectively and the kinetic energy of the Sn $M_4N_{4,5}N_{4,5}$ Auger line was 428.5 eV. The modified Auger parameter (*30*) of Sn was calculated to be 919.0 eV. These values were independent of the catalyst composition and consistent with those for pure SnO_2 and MoO_3 catalysts within the accuracy of ±0.2 eV.

The surface composition of the catalyst was obtained from the XPS area intensities of the Mo_{3d} and $Sn_{3d_{5/2}}$ bands and summarized in Table 1. Figure 2 shows the surface composition of the catalyst as a function of the bulk one. Although the surface composition is not equilibrated with the bulk one under the present preparation conditions, it is evident that the surface enrichment of Mo occurs in the region of R_B[1] = Mo/Mo + Sn < 0.75, whereas the superficial segregation of Sn occurs in the other region. A relationship similar to that in Fig. 2 has been previously reported for SnO_2–MoO_3 catalysts prepared by calcining mixtures of SnO_2 and MoO_3 (*1*). Although no datum on

[1] R_B and R_S denote Mo/Mo + Sn atomic ratios in bulk and in surface of SnO_2–MoO_3 catalysts, respectively, hereafter.

TABLE 1

Surface Properties of SnO_2–MoO_3 Catalysts

Bulk composition[a] (R_B = Mo/Mo + Sn)	Surface area (m^2/g)	Surface composition (R_S = Mo/Mo + Sn)[a]		
		Fresh[b]	After reaction[c]	After reduction[d]
0	8.2	0	0	0
0.05	30.5	0.15	0.17	0.15
0.1	33.4	0.23	0.26	0.26
0.2	74.1	0.35	0.40	0.38
0.3	45.8	0.45	0.53	
0.4	83.5	0.47	0.56	
0.5	9.7	0.60	0.60	0.63
0.6	17.5	0.69	0.71	0.79
0.7	13.2	0.71	0.72	
0.8	21.8	0.75	0.78	
0.9	12.1	0.88	0.89	
1.0	1.6	1.0	1.0	

[a] Atomic ratio.
[b] Calcined at 550°C for 5 h in air.
[c] *sec.*-Butyl alcohol conversion at 190°C in an air stream for 1.5 h (alcohol/O_2; 1.16).
[d] Reduced with *sec.*-butyl alcohol at 190°C for 1.5 h (alcohol flow rate; 0.109 mol/h · g cat.).

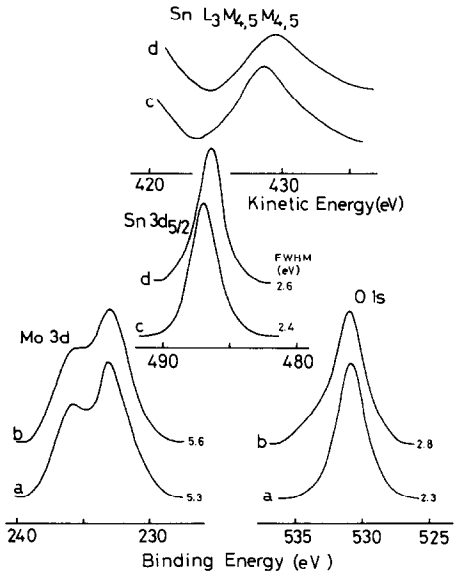

FIG. 1. X-Ray photoelectron spectra of the Mo_{3d}, O_{1s}, $Sn_{3d_{5/2}}$ levels and Auger spectra of the Sn $M_4N_{4,5}N_{4,5}$ level for SnO_2–MoO_3 catalysts calcined at 550°C; (a) R_B = 0.2, fresh; (b) R_B = 0.2, after the reaction of *sec.*-butyl alcohol in an air stream at 190°C for 1.5 h; (c) R_B = 0.9, fresh or after the *sec.*-butyl alcohol reaction in an air stream; (d) R_B = 0.9, reduced with H_2 at 400°C for 1 h.

the surface free energy of SnO_2 is available, it is deduced that the Mo enrichment in the surface is induced by thermodynamic requirements, taking into consideration the extremely low surface free energy of MoO_3 (50–70 ergs/cm^2) (*6*) compared to other metal oxides, such as PbO (130–150 ergs/cm^2), and GeO_2 (ca. 200 ergs/cm^2) (*6*). In contrast, the surface enrichment of Sn in the Mo-rich catalysts may be a consequence of exclusion effects due to the crystallization of MoO_3, which develops rapidly in this composition range as shown below

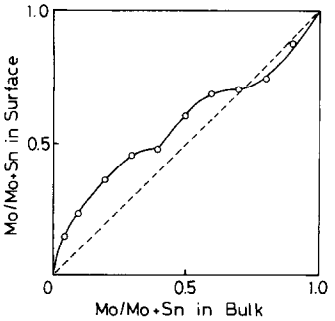

FIG. 2. Correlation between surface and bulk compositions of SnO_2–MoO_3 catalysts calcined at 550°C.

(Figs. 8 and 9). Similar observations were made for Co–Mo (*8*) and Sn–Zr (*2*) mixed oxide catalysts. A small concavity around $R_B = 0.4$ is due to a change in the surface structure of the SnO_2–MoO_3 catalysts with the catalyst composition, accompanied by an abrupt surface area change of the catalyst as shown in Table 1. Since no mixed oxide compound is found, it is assumed that the surface enrichment of Mo or Sn in the catalysts with $R_B > 0.4$ indicates the larger fraction of surface area of Mo or Sn oxide than that expected from the bulk composition. More surface-sensitive techniques, such as ISS, would provide more precise surface structure, if combined with scanning AES techniques.

The catalytic conversion of *sec.*-butyl alcohol (2-BA) was carried out over the SnO_2–MoO_3 catalysts at 190°C in an air stream. After the catalyst had reached a steady activity, X-ray photoelectron spectra of the catalyst were measured without exposing it to air. Figure 1 shows typical Mo_{3d}, $Sn_{3d_{5/2}}$, Sn *MNN* Auger, and O_{1s} spectra. The binding energies of the $Mo_{3d_{5/2}}$ and $Sn_{3d_{5/2}}$ bands and kinetic energy of the Sn *MNN* Auger lines did not show any appreciable shifts. However, the linewidth of the Mo_{3d} level showed some broadening, indicating a slight reduction of Mo(VI) during the reaction. On the other hand, no such change was observed for the Sn spectra. The surface composition of the catalyst was found to be slightly altered by the reaction as shown in Table 1, that is, slight surface enrichments of Mo are evidently induced by the reaction. The reduction and superficial enrichment of Mo imply that Mo is responsible for the reaction. As for the O_{1s} spectra, a weak shoulder at ca. 533 eV appeared after the reaction (Fig. 1), indicating the formation of surface hydroxyl groups, since the shoulder at ca. 533 eV was also observed when SnO_2–MoO_3 catalysts were reduced with H_2 at 400°C.

Figure 3 shows the catalytic activities of the SnO_2–MoO_3 catalysts for the formations of the ketone and butenes as a function of the surface composition of the fresh catalyst. Of interest in Fig. 3 are the facts that the catalyst shows two activity maxima for both the dehydrogenation and dehydration of the alcohol at $R_S = 0.25$ and 0.70 and that in the Sn-rich region, the activities for both reactions are comparable, while in the Mo-rich region, the dehydration is much more prominent. In contrast to the present observations, Okamoto *et al.* (*1*) reported with the SnO_2–MoO_3 catalysts prepared by calcining mechanical mixtures of SnO_2 and MoO_3 catalysts prepared by calcining mechanical mixtures of SnO_2 and MoO_3 that a single maximum was present around the surface composition of $R_S = 0.5$ and that the dehydration activity was much higher than the dehydrogenation activity for the 2-BA conversion. The differences in the catalytic behavior among previous and present catalyst systems, that is, preparation effects are discussed below in terms of the catalyst structure.

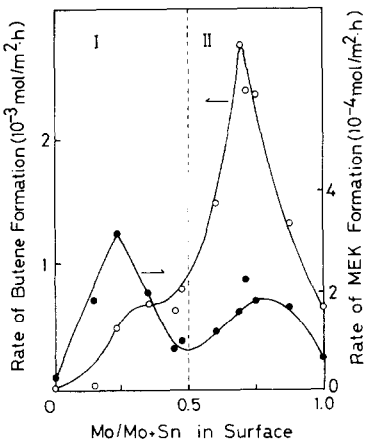

FIG. 3. Catalytic activities of SnO_2–MoO_3 catalyst to the formations of butenes and methylethylketone (MEK) in the conversion of *sec.*-butyl alcohol as a function of the surface composition (R_S) of the fresh catalyst. Reaction temperature: 190°C, *sec.*-butyl alcohol/O_2 = 1.16, feed rate of the alcohol: 1.09×10^{-2} mol/h. I and II show two groups of the catalyst; catalyst I and catalyst II.

For convenience, we classify the SnO_2–MoO_3 catalysts into two groups in terms of the surface composition as shown in Fig. 3; catalyst-I ($R_S < 0.5$ or $R_B < 0.4$) and

catalyst-II ($R_S > 0.5$ or $R_B > 0.4$). The catalytic conversion of 2-BA in a N_2 stream (in the absence of oxygen) revealed that the dehydrogenation activity of catalyst I decreased by 80% or more after 1.5-h reaction compared to that in the air stream, whereas that of catalyst II only by ca. 20%. In both catalyst systems, the dehydration activity decreased by ca. 20%. These results indicate that the dehydrogenation activity of catalyst I is mainly oxidative (>80%), while that of catalyst II is nonoxidative and attributable to a simple dehydrogenation over basic and acidic sites.

To examine these differences further, the reduction of the catalyst with 2-BA was carried out at 190°C by replacing the air stream with a N_2 stream. After the reduction for 1.5 h, the XPS spectra of the catalyst were measured without exposing it to air or moisture. Some typical Mo_{3d} spectra are shown in Fig. 4. The binding energies of the $Mo_{3d_{5/2}}$ band for catalyst I shifted from 233.1 to 231.9 eV, while the Mo_{3d} bandwidths remained rather narrow (FWHM = ca. 5.8 eV compared to 5.3 eV for the fresh catalysts). Accordingly, the resultant Mo_{3d} spectra cannot be understood in terms of simple superpositions of Mo(VI) ($Mo_{3d_{5/2}}$; 233.1 eV) and Mo(IV) (229.9 eV) spectra, implying the formation of a new Mo species with the binding energy of 231.9 eV. On the contrary, the Mo_{3d} spectra for catalyst II became unresolved when exposed to the alcohol, while the $Mo_{3d_{5/2}}$ energies were still ca. 233 eV. This indicates that only a small fraction of Mo(VI) was reduced to lower valent states.

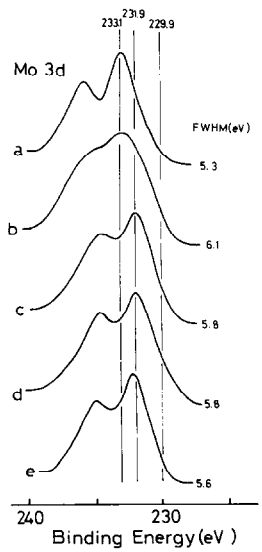

FIG. 4. X-Ray photoelectron spectra of the Mo_{3d} level for SnO_2–MoO_3 catalysts reduced with *sec.*-butyl alcohol (0.109 mol/h · g cat.) at 190°C for 1.5 h. (a) Pure MoO_3, (b) $R_B = 0.6$, (c) $R_B = 0.2$, (d) $R_B = 0.1$, and (e) $R_B = 0.05$ catalysts.

The new Mo species having the binding energy (231.9 eV) intermediate between Mo(VI) and Mo(IV) is undoubtedly ascribable to Mo(V). According to Patterson *et al.* (*31*), the $Mo_{3d_{5/2}}$ binding energies for Mo(VI), Mo(V), and Mo(IV) in reduced MoO_3/Al_2O_3 catalysts were reported to be 233.0, 231.9, and 229.9 eV, respectively. Ward and co-workers (*32*) showed the same values for MoO_3 supported on SiO_2. Nikishenko *et al.* (*33*) also reported the Mo(V) binding energies of 231.8 and 231.6 eV for reduced MoO_3 and CoO–MoO_3 catalysts supported on Al_2O_3, respectively. Vedrine *et al.* (*34*) showed 1.4 eV lower $Mo_{3d_{5/2}}$ energy for Mo(V) compared to that for Mo(VI) with Mo dissolved in TiO_2 lattice. Our assignment is strongly supported by their results.

It is noteworthy that on contact with 2-BA, a substantial amount of Mo(VI) in catalyst I is reduced almost exclusively to Mo(V), while only a small part of Mo(VI) in catalyst II to Mo(V) and/or Mo(IV). This is in good agreement with the fact that the oxidative dehydrogenation of 2-BA occurs in catalyst I, whereas the nonoxidative one takes place in catalyst II. As for the pure MoO_3 catalyst, neither chemical shift nor broadening of the Mo_{3d} level were observed when contacted with 2-BA in the air or N_2 stream. This indicates that Mo oxide in the mixed catalysts is activated by the presence of SnO_2.

To characterize further the properties of surface Mo in the catalyst, H_2 reductions of the catalysts were undertaken in flowing H_2

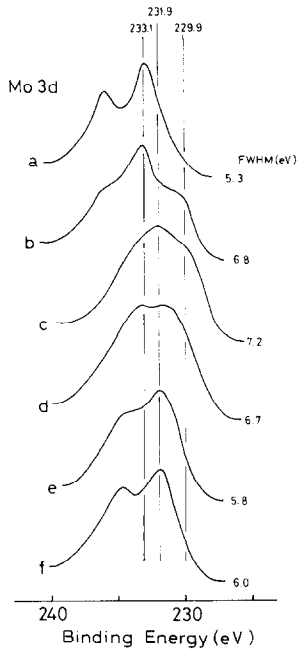

FIG. 5. X-Ray photoelectron spectra of the Mo_{3d} level for SnO_2–MoO_3 catalysts reduced with H_2 at 400°C for 1 h. (a) Pure MoO_3, (b) $R_B = 0.9$, (c) $R_B = 0.6$, (d) $R_B = 0.4$, (e) $R_B = 0.1$, and (f) $R_B = 0.05$ catalysts.

at 400°C and atmospheric pressure. The X-ray photoelectron spectra of the Mo_{3d} level are shown in Fig. 5 for the catalysts reduced for 1 h. It is surprising that the oxidation state of Mo in catalyst I ($R_S < 0.5$ or $R_B < 0.4$) is still mainly pentavalent in spite of the H_2 reduction. These findings lead us to the conclusion that in catalyst I, Mo(V) is easily produced under the mild reduction conditions (at 190°C with 2-BA), whereas it is very stable for further reduction even under the rather severe conditions (at 400°C with H_2). In contrast, a considerable amount of Mo(IV) (229.9 eV) was formed in the case of catalyst II ($R_S > 0.5$ or $R_B > 0.4$) when reduced with H_2, as shown in Fig. 5. Some Mo(VI) species remained intact after the H_2 reduction. The unreduced Mo oxide is unambiguously attributable to crystalline MoO_3 not activated by SnO_2, since pure MoO_3 catalyst did not suffer any appreciable reduction by H_2 under the same conditions. Therefore, it is concluded that catalyst II consists of two kinds of Mo phase; crystalline MoO_3 phase which is reduced by neither 2-BA nor H_2 and Mo oxide phase which is easily reduced by H_2 but slightly by 2-BA. The crystalline MoO_3 phase would be reduced by H_2 on a prolonged exposure after a well-known induction period. Consequently, the lattice oxygens in these two groups of the SnO_2–MoO_3 catalysts are significantly different in their reactivity, this resulting in the apparent differences in their catalytic behavior.

With the behavior of Sn in these catalysts, neither the chemical shift of the $Sn_{3d_{5/2}}$ band nor the change in the modified Sn Auger parameter were observed when the catalysts were contacted with 2-BA in the air or N_2 stream (Fig. 1), suggesting that only the lattice oxygen attached to Mo is responsible for the dehydrogenation of the alcohol. Hydrogen reduction of the Mo-rich catalyst (catalyst II) showed that the binding energy of the $Sn_{3d_{5/2}}$ level shifted to lower value by ca. 0.4 eV and that the modified Auger parameter changed to 920.0 eV, indicating clearly the reduction of Sn(IV) to Sn(II) (*1, 30, 35, 36*). However, in the case of Sn-rich catalysts (catalyst I), no appreciable reduction of Sn was observed. To confirm the XPS observations, Mössbauer spectra of the catalysts were measured. As shown in Fig. 6 ($R_B = 0.6$ catalyst), a new weak peak appeared at ca.

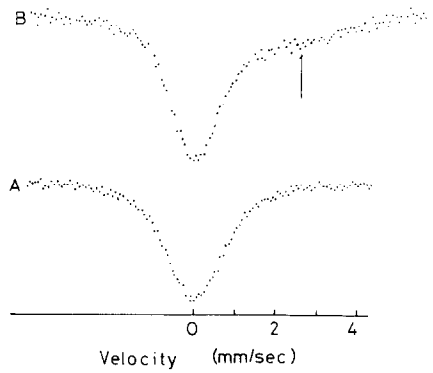

FIG. 6. Mössbauer spectra of Sn for SnO_2–MoO_3 catalyst ($R_B = 0.6$); (A) fresh or contacted with *sec.*-butyl alcohol at 190°C for 1.5 h in a N_2 stream, and (B) reduced with H_2 at 400°C for 1 h.

2.7 mm/sec only for catalyst II when reduced with H_2 at 400°C. The new peak is apparently attributable to Sn(II) (*17*). Combining the XPS and Mössbauer results, it is suggested that only the superficial reduction of Sn oxide phase occurs in catalyst II when reduced with H_2. Accordingly, the reactivities of lattice oxygens in both Sn and Mo oxide phases are greatly enhanced by combining the two component oxides.

ESR spectra of the SnO_2–MoO_3 catalysts (R_B = 0.1 and 0.7 catalysts for typical catalyst I and II, respectively) were measured to access the behavior of Mo(V) in the reduction with 2-BA and compared with the XPS results. The ESR signal due to Mo(V) species were observed at g = 1.930 ($\Delta H \doteqdot$ 100 G) for the fresh and reduced catalysts. Figure 7 illustrates the changes in the Mo(V) ESR intensity with the reduction time at 250°C. Since the line width of the signal did not vary with the reduction, a peak-to-peak intensity was taken as a Mo(V) concentration in the catalyst. In Fig. 7, the ESR intensities for reduced catalysts are normalized to those for the corresponding fresh catalysts. Unexpectedly, the ESR intensity for catalyst I (R_B = 0.1) decreased

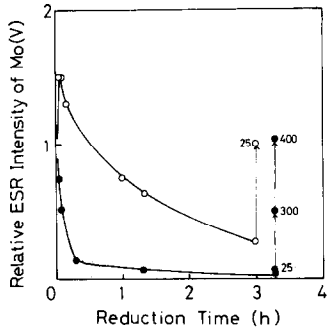

FIG. 7. Changes in the relative ESR intensity of Mo(V) with the reduction time (h) for SnO_2–MoO_3 catalysts (○, R_B = 0.1; and ●, R_B = 0.7). ESR intensities for the reduced catalysts are normalized to those for the corresponding fresh catalysts. Reduction was carried out at 250°C with 10 Torr of *sec.*-butyl alcohol, followed by evacuation before ESR measurements. Vertical lines indicate the ESR intensities for the reduced catalysts treated successively with 150 Torr of O_2 at the indicated temperatures for 30 min.

with increasing the contact time with the alcohol after taking a maximum at a very short reduction time. After the 3-h contact, the XPS spectra of the catalyst showed a considerable formation of Mo(V), Therefore, these results may imply strong interactions between Mo(V) ions (*37–39*). With catalyst II the ESR intensity decreased more rapidly on the reduction with 2-BA compared to catalyst I. In this case, some reduction of Mo(V) to Mo(IV) cannot be excluded in addition to the interactions between Mo(V) ions, since Mo(IV) is relatively easily produced in catalyst II. In both catalyst systems, no ESR signal ascribable to Sn(III) (*40*) was detected.

As for the interactions between gaseous O_2 and reduced Mo, the ESR signal intensity of Mo(V) in catalyst I immediately recovered to the original value when 150 Torr of O_2 was introduced into the reduced catalyst at room temperature, as shown in Fig. 7. In contrast, the Mo(V) signal in catalyst II reached the value of the fresh catalyst only when treated with O_2 at 400°C. These differences in the redox properties of Mo between catalyst I and II would result from the differences in the catalyst structure.

In order to examine the structure of the SnO_2—MoO_3 catalysts, the ir intensity of the Mo=O band and XRD intensities of crystalline MoO_3 and SnO_2 were measured. The position of the Mo=O band (990 cm^{-1}) did not change with the catalyst composition within ±3 cm^{-1} and was identical to that for pure MoO_3. The Mo=O band intensity was referenced to the υ_1 band (1100 cm^{-1}) of $MgCO_3$. The I_{990}/I_{1100} values are plotted in Fig. 8 as a function of the bulk composition of the catalyst. Figure 9 shows the crystallinities of MoO_3 and SnO_2 relative to the reference, silicon. The crystallite size of MoO_3 calculated from XRD line broadenings was 36 ± 4 nm for the catalysts with $R_B \geq 0.6$ and decreased with decreasing the MoO_3 content (20 nm at R_B = 0.3), while that of SnO_2 decreased sharply from 15 nm (pure SnO_2) to 4 nm ($R_B \leq 0.2$) and

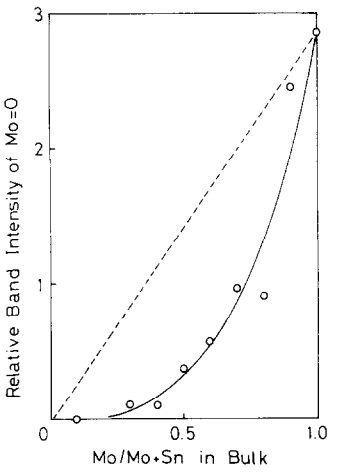

FIG. 8. Relative ir-band intensity of Mo═O for SnO_2—MoO_3 catalyst as a function of Mo/Mo + Sn atomic ratio in bulk. Dashed line indicates a Mo═O band intensity expected from the bulk composition of the catalyst.

was maintained constant for further increase in the MoO_3 content.

From Figs. 8 and 9, it is evident that the Mo═O double bond comes from crystalline MoO_3 and that the crystallinity of MoO_3 in the catalyst, particularly in catalyst I, is significantly decreased by the presence of Sn oxide compared to that expected from the catalyst composition (dashed line). Taking into account the differences in the reduction and oxidation behaviors of Mo(VI) and Mo(V) among catalyst I, II, and pure MoO_3, as well the results in Fig. 8 and 9, it is considered that in catalyst I, Mo is dissolved into substitutional positions of SnO_2 lattice, whereas in catalyst II, the crystal structure of MoO_3 is considerably disturbed by the contact with Sn oxide to form amorphous Mo oxide in the boundary layers. The abrupt decrease in the crystallinity of SnO_2 at a low MoO_3 content (catalyst I, Fig. 9) would be resulted from the dissolution of Mo into substitutional positions in the SnO_2 lattice.

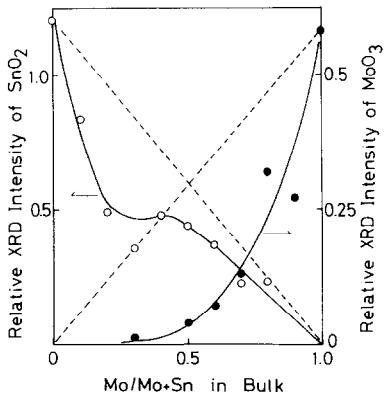

FIG. 9. Relative crystallinities of MoO_3 (●) and SnO_2 (○) in SnO_2–MoO_3 catalyst as a function of Mo/Mo + Sn atomic ratio in bulk. Dashed lines indicate the correlations expected from the bulk composition of the catalyst.

The possibility of Mo dissolution into substitutional positions in SnO_2 lattice was claimed by Meriaudeau *et al.* (*41*) using ESR. They also showed the Mo(V) in the SnO_2 lattice was stabilized for further reduction. This behavior of Mo(V) is completely consistent with our observations. SnO_2–MoO_3 mixed oxide catalysts prepared by calcining the mixtures of SnO_2 and MoO_3 showed only the catalytic properties of catalyst II (*1*). These facts provide further evidence for the activation processes in the combination of two composite oxides.

In the dissolution model, the charge balance may be achieved by the delocalization of the extra electrons in conduction band and partly by the localization in Mo(VI) ions to form Mo(V), since no detectable amounts of Mo(IV), Sn(III), and Sn(II) were observed by means of XPS, ESR, and Mössbauer spectroscopies. The latter possibility is evidenced by 10–15 times higher Mo(V) ESR intensities per Mo for $R_B \leq 0.1$ catalysts compared to those for $R_B > 0.2$ catalysts. The possibility of the former process was claimed by Portefaix *et al.* (*42*) for Sb(V) in SnO_2 lattice.

With increasing the Mo content up to R_B = ca. 0.1, the amount of Mo dissolved in substitutional positions of SnO_2 lattice increases and reaches the maximum, where 25% of Sn ions in the surface are replaced by Mo(VI) ions ($R_S = 0.25$). This value may indicate the maximum capacity of Mo dis-

solution into SnO_2 lattice in the surface, forming a stable surface phase. Cross and Pike (*11*) have suggested for Sb–Sn mixed oxide catalysts that Sb(V) is dissolved into the substitutional positions of SnO_2 lattice up to Sb/Sb + Sn = 0.25 in surface. The maximum capacity for Sb dissolution is identical to that for Mo. This agreement is not surprising, since the ionic radii for Mo(VI) and Sb(V) are the same (0.062 nm) (*43*).

Further increase in the surface Mo content up to R_S = ca. 0.5 would induce the segregation of Mo from the SnO_2 lattice to form biphasic mixtures; pure Mo and Sn oxides. This is clearly evidenced by the increase in the crystallinity of SnO_2 as shown in Fig. 9. This process is accompanied by the decrease in the oxidative dehydrogenation activity of the catalyst. Nevertheless, the properties of catalyst II is not yet developed around R_S = 0.5 because of a small amount of MoO_3 phase compared to SnO_2. In the composition range corresponding to catalyst II, the maximum activity and thus maximum acidity and basicity are determined by the maximum contact area between SnO_2 and MoO_3 particles, which depends strongly both on the relative particle or crystallite sizes of SnO_2 and MoO_3 (about 4 and 36 nm, respectively, in the present catalysts) and on the amounts of the component oxides. Accordingly, the activity and selectivity of the SnO_2–MoO_3 catalyst for the 2-BA conversion in Fig. 3 can be understood in terms of the transformations of the surface structure with the catalyst composition.

In order to examine the reaction mechanism of the oxidative dehydrogenation of alcohols over catalyst I, the reduction experiments of the R_B = 0.1 catalyst were carried out using C_1–C_5 alcohols (C_1; methyl alcohol, C_2; ethyl alcohol, C_3; *n*-propyl alcohol, C_4; 2-BA, and C_5; *n*-pentyl alcohol). Figure 10 shows the X-ray photoelectron spectra of the Mo_{3d} and O_{1s} levels after a 1.5-h reduction in the flowing alcohol at 190°C. It appears that with increasing

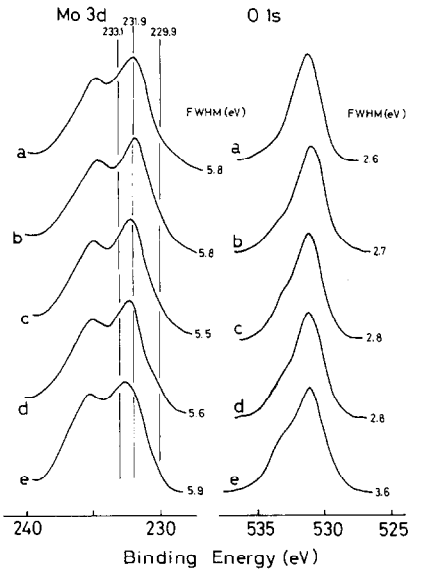

FIG. 10. X-Ray photoelectron spectra of the Mo_{3d} and O_{1s} levels for the R_B = 0.1 catalyst after reduced with the alcohol (0.109 mol/h · g cat.) in a N_2 stream at 190°C for 1.5 h; (a) *n*-pentyl alcohol, (b) *sec.*-butyl alcohol, (c) *n*-propyl alcohol, (d) ethyl alcohol, and (e) methyl alcohol.

carbon number of the alcohol, the extent of reduction of Mo(VI) to Mo(V) increases, while the intensity of the new O_{1s} XPS peak (ca. 533 eV), which is ascribable to surface hydroxyl groups, and probably, to alkoxide groups, decreases. The reactivity of the alcohol increased with the carbon number. These results suggest the reaction mechanism in Fig. 11, where the α-H abstraction from the alkoxide group is assumed to be a rate-determining step. In this reaction scheme, the structure of active sites is supposed to be paired Mo(VI) atoms surrounded by Sn(IV) atoms. The Mo(VI) atoms are finally reduced to the Mo(V) state upon the dehydrogenation of the alcohol. In this reaction mechanism, the role of Sn is restricted to provide active Mo species by dissolution into the SnO_2 lattice. However, it cannot be ruled out that the redox cycle of Sn, such as Sn(IV)–Sn(II), participates to some extent in the reaction, although no reduction of Sn(IV) to Sn(II) was explicity detected here on the contact with the alcohol or H_2. Such redox process

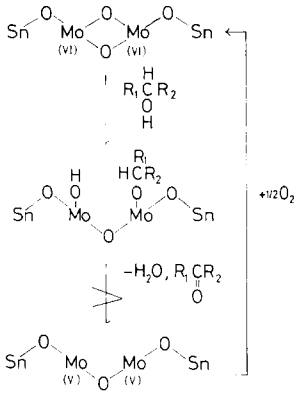

FIG. 11. Possible reaction mechanism for the oxidative dehydrogenation of alcohol over catalyst I.

might catalyze the reoxidation of Mo(V) to Mo(VI) with gaseous O_2.

As shown above, the reactivity of lattice oxygen in catalyst I and II are considerably different for the conversion of 2-BA. The lattice oxygen in catalyst I is active for the oxidative dehydrogenation of alcohols. These results remind us the dependencies of the activities of SnO_2–MoO_3 catalysts for the oxidative dehydrogenation of butene to butadiene and for maleic anhydride formation in butadiene oxidation upon the composition of the catalyst (*25*). The former reaction showed a maximum at ca. 10% Mo in bulk, whereas the latter at ca. 60% Mo. Ai (*25*) explained the results in terms of the acid–base properties of the catalyst. However, it is interesting to conjecture that these selectivities of the catalyst result from the differences in the reactivity of lattice oxygen toward the dehydrogenation and the oxygen-additive reactions as well as the solid acid–base properties of the catalyst, since these activity maxima correspond to good catalyst I and II, respectively. Nevertheless, the explanation is hypothetical now and needs further verification.

CONCLUSIONS

Characterization of SnO_2–MoO_3 catalysts were undertaken using XPS, ir, XRD, ESR, and Mössbauer spectroscopy and compared with the reaction of *sec.*-butyl alcohol over the catalysts. SnO_2–MoO_3 catalysts were classified into two groups in terms of the catalytic properties; catalyst I (Mo/Mo + Sn < 0.5 in surface) and catalyst II (Mo/Mo + Sn > 0.5). The salient findings in this study are as follows:

(1) a surface enrichment of Mo was observed in the bulk composition of Mo/Mo + Sn < 0.75 and a Sn enrichment in the other region,

(2) catalyst I shows comparable dehydrogenation and dehydration activities, whereas catalyst II much higher dehydration activity than dehydrogenation,

(3) Mo(VI) in catalyst I is easily reduced to Mo(V) on a contact with the alcohol at 190°C and the Mo(V) is stable against further reduction by a H_2 treatment at 400°C,

(4) in contrast, Mo(VI) in catalyst II is hardly reduced with the alcohol but partially reduced to Mo(IV) with H_2,

(5) Mo(V) in catalyst I is easily oxidized to Mo(VI), whereas Mo(V) and Mo(IV) in catalyst II are difficult to be oxidized with gaseous O_2,

(6) in catalyst I, Mo is suggested to be dissolved into substitutional positions in SnO_2 lattice, and

(7) in catalyst II, Mo and Sn oxides are suggested to be activated by mutual contacts between them, forming active amorphous phases in the grain boundaries.

In this study on SnO_2–MoO_3 catalysts, two activation modes of lattice oxygen were suggested to interpret the synergetic effects between SnO_2 and MoO_3 and correlated with catalytic properties. These activation processes of lattice oxygen would operate in other mixed oxide systems as well as mixed compound formations.

ACKNOWLEDGMENT

We extend our thanks to Professor T. Shinjo (Institute of Chemistry, Kyoto University) for the measurements of Mössbauer spectra of the catalyst.

REFERENCES

1. Okamoto, Y., Hashimoto, T., Imanaka, T., and Teranishi, S., *Chem. Lett.*, 1035 (1978).

2. Imanaka, T., Hashimoto, T., Sakurai, K., Okamoto, Y., and Teranishi, S., *Bull. Chem. Soc. Japan* **53**, 1206 (1980).
3. Matsuura, I., Schut, R., and Hirakawa, K., *J. Catal.* **63**, 152 (1980).
4. Herniman, H. J., Pyke, D. R., and Reid, R., *J. Catal.* **58**, 68 (1979).
5. Boudeville, Y., Figueras, F., Forissier, M., Portefaix, J., and Vedrine, J., *J. Catal.* **58**, 52 (1979).
6. Overbury, S. H., Ertrand, P. A., and Somorjai, G. H., *Chem. Rev.* **75**, 547 (1975).
7. Cimino, A., Minelli, G., and DeAngelis, B. A., *J. Electron Spectrosc. Relat. Phenom.* **13**, 291 (1978).
8. Menon, P. G. and Prasad Rao, T. S. R., *Catal. Rev.* **20**, 97 (1979).
9. Okamoto, Y., Shimokawa, T., Imanaka, T., and Teranishi, S., *J. Catal.* **57**, 153 (1979).
10. Andersson, S. L. T., *J. Chem. Soc. Faraday Trans. I* **75**, 1356 (1979).
11. Cross, Y. M. and Pyke, D. R., *J. Catal.* **58**, 61 (1979).
12. Aso, I., Amamoto, T., Yamazoe, N., and Seiyama, T., *Chem. Lett.*, 365 (1980).
13. Okamoto, Y., Shimokawa, T., Imanaka, T., and Teranishi, S., *J. Chem. Soc. Chem. Commun.*, 47 (1978).
14. Haber, J., Stoch, J., and Wiltowski, T., *React. Kinet. Catal. Lett.* **13**, 161 (1980).
15. Grzybowska, B., Haber, J., Marczewski, W., and Ungier, L., *J. Catal.* **42**, 327 (1976).
16. Margolis, L. Ya., Krylov, O. V., and Isaev, O. V., *in* "Proceedings, 5th International Congress on Catalysis," p. 1039, 1972.
17. Margolis, L. Ya., *J. Catal.* **21**, 93 (1971).
18. Morooka, Y., and Takita, Y., *in* "Proceedings, 5th International Congress on Catalysis," p. 1025, 1972.
19. Takita, Y., Ozaki, A., and Morooka, Y., *J. Catal.* **27**, 185 (1972).
20. Morooka, Y., Takita, Y., and Ozaki, A., *J. Catal.* **23**, 183 (1971).
21. Tan, S., Morooka, Y., and Ozaki, A., *J. Catal.* **17**, 132 (1970).
22. Buiten, J., *J. Catal.* **10**, 188 (1968).
23. Buiten, J., *J. Catal.* **13**, 378 (1969).
24. Buiten, J., *J. Catal.* **27**, 232 (1972).
25. Ai, M., *J. Catal.* **40**, 327 (1975).
26. Niwa, M., Mizutani, M., and Murakami, Y., *Chem. Lett.*, 1295 (1975).
27. Ai, M., *J. Catal.* **54**, 426 (1978).
28. Wagner, C. D., *Anal. Chem.* **44**, 1050 (1972).
29. Okamoto, Y., Tomioka, H., Katoh, Y., Imanaka, T., and Teranishi, S., *J. Phys. Chem.* **84**, 1833 (1980).
30. Wagner, C. D., Gale, L. H., and Raymond, R. H., *Anal. Chem.* **51**, 466 (1979).
31. Patterson, T. A., Carver, J. C., Leyden, D. E., and Hercules, D. M., *J. Phys. Chem.* **80**, 1700 (1976).
32. Ward, M. B., Lin, M. J., and Lunsford, J. H., *J. Catal.* **50**, 306 (1977).
33. Nikishenko, S. B., Slinkin, A. A., Shipiro, E. S., Antoshin, G. V., and Minachev, Kh. M., *Kinet. Catal.* **20**, 432 (1979).
34. Vedrine, J. C., Praliaud, H., and Meriaudeau, P., *Surface Sci.* **80**, 101 (1979).
35. Wagner, C. D., and Biloen, P., *Surface Sci.* **35**, 82 (1973).
36. Okamoto, Y., Carter, W. J., and Hercules, D. M., *Appl. Spectrosc.* **33**, 287 (1979).
37. Hall, W. K., and LoJacono, M., *in* "Proceedings, 6th International Congress on Catalysis," p. 246, 1977.
38. Abdo, S., Clarkson, R. B., and Hall, W. K., *J. Phys. Chem.* **80**, 2431 (1976).
39. Hare, C. R., Bernal, I., and Gray, H. B., *Inorg. Chem.* **1**, 831 (1962).
40. Itoh, M., Hattori, H., and Tanabe, K., *J. Catal.* **43**, 192 (1976).
41. Meriaudeau, P., Che, M., and Tench, A. J., *Chem. Phys. Lett.* **31**, 547 (1975).
42. Portefaix, J. L., Bussiere, P., Forissier, M., Figueras, F., Friedt, J. M., Sanchez, J. P., and Theobald, F., *J. Chem. Soc. Faraday Trans. I* **76**, 1652 (1980).
43. "Handbook of Chemistry and Physics," 46th ed. The Chemical Rubber Co., Cleveland, 1966.